Computational Decision Support for Percutaneous Aortic Valve Implantation

Ingmar Voigt[1,3] ⋆, Razvan Ioan Ionasec[2,4], Bogdan Georgescu[2], Jan Boese[5], Gernot Brockmann[6], Joachim Hornegger[5], and Dorin Comaniciu[2]

[1] Software and Engineering, Siemens Corporate Technology, Erlangen, Germany
[2] Integrated Data Systems, Siemens Corporate Research, Princeton, USA
[3] Pattern Recognition Lab, Friedrich-Alexander-University, Erlangen, Germany
[4] Computer Aided Medical Procedures, Technical University Munich, Germany
[5] Siemens Healthcare, Angiography & X-Ray-Systems, Forcheim, Germany
[6] German Heart Center Munich

Abstract. Valve replacement is the most common therapy for diseased aortic valves. Percutaneous approaches are becoming increasingly popular, due to reduced procedural complications and lower follow-up rates. Still there is a lack of efficient tools for valve quantification and preoperative simulation of replacement and repair procedures. Thus the success of the intervention relies to a large portion on experience and skills of the operator. In this paper we propose a novel framework for preoperative planning, intraoperative guidance and post-operative assessment of percutaneous aortic valve replacement procedures with stent mounted devices. A comprehensive model of the aortic valvular complex including aortic valve and aorta ascendens is estimated with fast and robust learning-based techniques from cardiac CT images. Consequently our model is used to perform a in-silico delivery of the valve implant based on deformable simplex meshes and geometrical constraints. The predictive power of the model-based in-silico valve replacement was validated on 3D cardiac CT data from 20 patients through comparison of preoperative prediction against postoperatively imaged real device. In our experiments the method performed with an average accuracy of 2.18 mm and a speed of 55 seconds. To the best of our knowledge, this is the first time a computational framework is validated using real pre- and postoperative patient data.

1 Introduction

Percutaneous aortic valve implantation (PAVI) has the potential to revolutionize the treatment of aortic valve disease, offering a less invasive alternative to open heart surgery. PAVI is already emerging as a feasible treatment for patients with high-surgical risk [1], over 30% of the symptomatic cases, and will account for 41.1% of the procedures by 2012 (Millennium Research Group 2008) [2]. The prosthetic implants are delivered through catheters using transvenous,

⋆ Correspondence to ingmar.voigt.ext@siemens.com

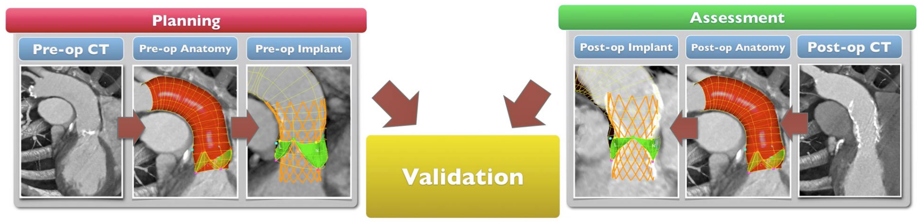

Fig. 1. Schematic description of the proposed PAVI computational decision support workflow.

transarterial or transapical techniques, while clinicians do not have direct view and access to the affected valve and surrounding anatomies.

Hence, critical decisions such as, type of procedure, implant type and sizing, deployment location and timing, and treatment assessment, are exclusively based on imaging techniques [3]. A misplaced implant can block the coronary ostia inducing a life threatening ischemic condition. Suboptimal deployment location can result in poor hemodynamic performance with severe paravalvular leakages and/or high gradients and suboptimal effective orifice. Wrong implant sizing may require re-operation or can damage the vessel tissue and cause catastrophic events as arterial dissection or rupture. Therefore advanced image analysis and computational models for precise planning, procedure guidance, and outcome assessment, may significantly improve percutaneous valve implantation techniques.

In this paper, we propose a computational framework for percutaneous aortic valve implantation, which supports decisions throughout the clinical workflow and is summarized in Sec. 2. Modeling of the aortic valve and ascending aorta and patient-specific estimation from pre- and post- operative cardiac CT images is described in Sec. 3. Sec. 4 presents the computational environment, which allows for in-silico valve implantation for evaluation and prediction of procedure success under various treatment scenarios. Comprehensive validation and performance evaluation is given in Sec. 5 by comparing the simulation results from preoperative data with the real device imaged in the postoperative data.

2 Computational Decision Support for PAVI

The proposed PAVI computational decision support workflow is illustrated in Fig. 1:

Pre-operative workflow: 1) Pre-operative cardiac CT volume acquisition for procedure planning purposes 2) Patient-Specific anatomical model estimation and automatic quantification for valve assessment and patient selection 3) In-silico valve implantation under various interventional procedure conditions for identification of optimal device type, size and deployment location as well as treatment outcome prediction until optimal predicted performance is observed.

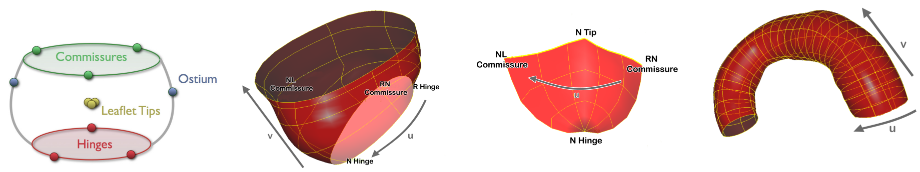

(a) (b) (c) (d)

Fig. 2. Aortic valve and ascending aortic root model. (a) shows a generic model of the aortic valve including nine anatomical landmarks. (b) shows our point distribution model of the aortic root. (c) presents the aorta leaflets model - the N leaflet is depicted. (d) demonstrates the ascending aortic root model. (e) represents the full model with the corresponding anatomical parameterization.

Post-operative workflow: 4) Post-operative cardiac CT volume acquisition for treatment evaluation 5) Patient-Specific anatomical model estimation for quantitative anatomical assessment 6) Patient-Specific deployed device estimation for quantitative implant assessment.

3 Patient-specific anatomical modeling and estimation

This section summarizes the anatomical model of the aortic valve and ascending aorta as well as the patient-specific estimation of its parameters from imaging data as in [4].

3.1 Aortic Valve and Ascending Aortic Root Modeling

The aortic root provides the supporting structures for the leaflets of the aortic valve and forms the bridge between the left ventricle and the ascending aorta. The root extends from the basal attachments of the leaflets, defined by the L (left) / R (right) / N (none) Hinges, to the sinutubular junction. The L / R / N aortic leaflets, are attached to the root on semilunar structures. Valve leaflets can be thought of as shirt pockets, with one edge stitched to the shirt and one free of attachment with is center marked by the L / R / N leaflet tips. These attachment structures interlink at the level of the sinutubular junction forming the LR / RN / NL commissures. The employed model represents the complete anatomy of the aortic valve and ascending aorta, which includes the aortic root, left / right / none aortic leaflets, ascending aorta and 11 anatomical landmarks.

Anatomical Landmarks: Represented by three-dimensional points in the Euclidean space, the considered anatomical landmarks are: L / R / N Hinges, LR / RN / NL commissures, L / R / N leaflet tips, and L / R coronary ostia.

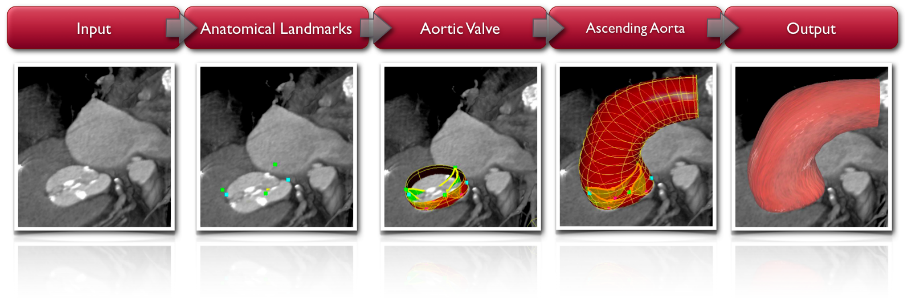

Fig. 3. A survey of our hierarchical model estimation schema.

Aortic valve root and leaflets: The aortic valve root is constrained by the commissures, hinges and ostia and represented as a tubular surface mesh. The mesh is aligned with the aortic circumferential u and ascending directions v and includes 36×10 vertices. The left / right / none aortic leaflets, are modeled as hyperbolic paraboloids on a grid of 11×7 vertices. Each leaflet is defined by one hinge, two commissures and one leaflet tip.

Ascending aortic root The ascending aorta emerges from the aortic root and incorporates a variable length. The anatomy is composed of a fixed number of circumferential coordinates $u = 36$ and a variable number of coordinates along the ascending direction v. The first ring starts at from the commissures.

3.2 Patient-Specific Model Estimation

The patient-specific parameters of the aortic valve and ascending aorta model described in Sec. 3.1 are estimated from volumetric images using a robust learning-based algorithm as in [5]. The a posteriori probability $p(M|I)$ of the model M given the image data I, is hierarchically estimated within the Marginal Space Learning (MSL) [6] framework. Detectors are successively trained using the Probabilistic Boosting Tree (PBT) [7] with Haar and Steerable features, and consequently applied to estimate the anatomical landmarks and structures from cardiac CT volumes as illustrated in Fig. 3. For further details the reader is referred to [4].

4 Device Modeling and In-Silico Deployment

4.1 Stent Model

A library of virtual devices/implants was created based on manufacturers' description to incorporate realistic geometrical properties. In this work two models of the CoreValve Revalving System by Medtronic (Minneapolis, MN, USA) are treated, namely the models CRS-P3-640 and CRS-P3-943 (Fig. 4(a)). The implant consists of 165 cells formed by the struts. The two models have length of 53 and 55 mm and diameters at the inflow, middle and outflow levels of 26, 22, 40 and 29, 24, 43 mm respectively. The Xenograft artificial valve consist of porcine pericardial tissue, out of which the leaflets are manufactured and mounted to the implant's stent. The library can be easily extended with future devices using the methods described in the following. The device is modeled out of two parts: a geometric representation, which precisely mimics the exact geometry of the device, the so-called *stent mesh*, and a second superimposed 2-simplex mesh, named in the following *computational mesh*, which is used for computation and to guide the expanding deformation [8, 9]. Fig. 4(b) depicts the topological relationship between the computational mesh and the stent mesh, which is composed of struts connecting a subset of points of the computational mesh. In order to infer the geometrical properties of the stent model various dimension were measured from stereolithographic scans of the modeled implants. These are the strut lengths, the characteristic angles in each cell and the device's circumferences at each level, where each level is defined by the strut joints.

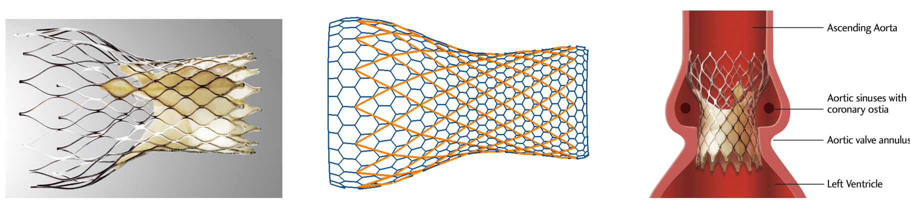

(a) (b) (c)

Fig. 4. (a) CoreValve implant, (b) long axis cross section of stent mesh (orange) with superimposed computational mesh (blue) and (c) CoreValve implant with sketch of target anatomy. (Sources a & c: http://www.medtronic.com)

4.2 Virtual Stent Deployment

To simulate valve replacement under various conditions, different devices are chosen from the library and virtually deployed under different parameters, into the previously extracted patient-specific model of the affected valve. The expansion of the device is modeled by balancing external and internal forces as encountered in the actual procedure, using iterative optimization methods. Following the works of Larrabide et. al. and Montagnat et. al. [8, 9], the expansion is described by a finite difference discretization of a second order differential equation:

$$\boldsymbol{p_i^{n+1}} = \boldsymbol{p_i^n} + (1-\gamma)(\boldsymbol{p_i^n} + \boldsymbol{p_i^{n-1}}) + f_{int}(\boldsymbol{p_i^n}) + f_{ext}(\boldsymbol{p_i^n}) + f_{reg}(\boldsymbol{p_i^n}) \tag{1}$$

where $\boldsymbol{p_i}$ is a point on the computational mesh, n is the iteration number, f_{ext}, f_{int} and f_{reg} external, internal and regularizing forces and the weighting parameter γ. Fig. 5 shows a visual description of each of the forces. An outline of the algorithm is given in Fig. 6. The internal forces $f_{int}(\boldsymbol{p_i^n}) = f_{length}(\boldsymbol{p_i^n}) + f_{angle}(\boldsymbol{p_i^n}) + f_{circ}(\boldsymbol{p_i^n})$ model the intrinsic properties of the stent and enforce deformation along it's surface normals and long axis as the device is self-expandable. Hence they are parameterized by strut lengths, characteristic angles and device circumferences, which were measured from the expanded template. Accordingly, these forces are adapted, such that the implant attempts to achieve the targeted dimensions, and they induce different expanding pressures at different levels. Particularly $f_{circ}(\boldsymbol{p_i^n}) = \boldsymbol{n}_i(c_k - \sum_{\forall j \in \mathcal{N}_k} ||\boldsymbol{p_j^n} - \boldsymbol{p_{j+1}^n}||)/2\pi$ pushes the points $\boldsymbol{p_i^n} \in \mathcal{N}_k$ along the surface normal $\boldsymbol{n}_i$ to satisfy the reference circumference c_k of the stent shape, where $\mathcal{N}_k$ is the set of strut joints at a level k. It is important to note, that f_{circ} does not enforce the stent diameter directly but the stent circumference instead to account for expansion into arbitrary shaped vessel geometries, which have typically non-circular cross sections. f_{length} and f_{angle} enforce the strut lengths and characteristic angles observed in the expanded shape [8]. The external forces $f_{ext}(\boldsymbol{p_i})$ model the interaction of stent and aortic valve and aorta tissue, and guide the implant deformation by balancing the internal device forces: $f_{ext}(\boldsymbol{p_i}) = -\boldsymbol{n}_i(\boldsymbol{n}_i \cdot f_{int}(\boldsymbol{p_i}))(||\boldsymbol{p_i^n} - \boldsymbol{c}_k||/||\boldsymbol{v} - \boldsymbol{c}_k||)$ with stent centroid $\boldsymbol{c}_k$ at level k and the intersection point $\boldsymbol{v}$ of normal and vessel surface. The regularizing forces f_{reg} are solely defined on the computational mesh to provide smoothness as described in [9]. As mentioned above the method focusses on self-expanding implants, which inherently exercise forces of minor amplitudes onto the surrounding vessel tissue. Therefore we argue, that the resulting minor deformations can be neglected.

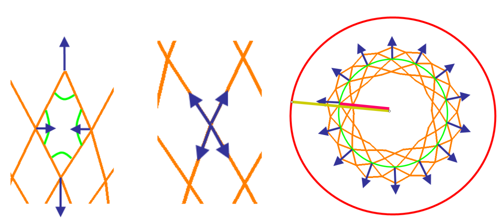

(a) (b) (c)

Fig. 5. Forces acting on the model on deployment to converge to the observed geometric properties: (a) f_{angle} enforces the charateristic angles at the strut joints (green), (b) f_{length} maintains the strut lengths. (c) f_{circ} enforces the circumference (green), while f_{ext} dampens and eliminates the all forces acting along the stent mesh normal wheighted by the fraction of distances of strut joint and vessel wall (red) to the stent centroid (magenta/yellow). Please note that (c) shows a short axis cross section of the stent mesh.

Input:

- Patient-specific model of aortic valve and aorta ascendens
- implant placement position and orientation

Output: Deployed Implant
Execute:

- create computational mesh and stent mesh with constant radius of 1 mm at manually selected placement position, oriented along the aortic root centerline
- **repeat:**
  - for each point $\boldsymbol{p}_i^n$ on the *computational mesh*, calculate $f_{reg}(\boldsymbol{p}_i^n)$, $f_{angle}(\boldsymbol{p}_i^n)$, $f_{length}(\boldsymbol{p}_i^n)$, $f_{circ}(\boldsymbol{p}_i^n)$ and $f_{ext}(\boldsymbol{p}_i^n)$
  - for each $\boldsymbol{p}_i^n$, compute $\boldsymbol{p}_i^{n+1}$ according to Eq. 1
  - if mean point displacement on the *stent mesh* $< \epsilon$, convergence achieved; stop execution

Fig. 6. The outline of our virtual stent deployment algorithm.

5 Experimental Results

The validation of the proposed framework is divided in two experiments. First we present results on the performance of the automatic patient-specific model estimation from pre- and post- cardiac CT data, as well as the quantitative variation between pre and postop ground truth anatomies, which is relevant for the subsequent virtual imlant deployment. Second we validate the proposed in-silico implantation, by comparing predicted valve deployment, using pre-operative data, with real deployment from post-operative data.

5.1 Validation of Patient-Specific Anatomical Modeling and Parameter Estimation

The data set used for patient-specific model estimation consists of 63 multi-phase (10 frames per cycle) cardiac CT and 21 single-phase cardiac CT acquisitions, which sums up to 651 CT volumes. Scans are acquired from different patients with various cardiovascular diseases (including ascending aortic root aneurysm, regugitation, calcific stenosis and bicuspid aortic valves), using different protocols, resulting in volumes with 80 to 350 slices and 153x153 up to 512x512 voxel grid resolution and 0.28mm to 2.0mm spatial resolution. Each data set is associated with an expert annotation used as ground-truth.

For the automatic patient-specific anatomical model estimation a combined accuracy of 1.45mm is obtained in 30sec on a standard desktop machine (Intel Xeon 2.66Ghz, 2GB RAM) for both pre- and post-operative volumes. Performance is reported on test data, which represents randomized 20% of the complete dataset, while the remaining 80% were used for training.

Due to different factors, a bias between the pre- and post-operative anatomical ground truth models can be expected. These are cardiac phase shifts and image noise but also deformation of the aortic vessel wall due to stent deployment, where the latter was assumed to be sufficiently small to be neglected in the deployment algorithm (Sec. 4.2). Therefore we quantified the differences for each pair of corresponding anatomical models obtained from a subset of 20 patients with pre- and postoperative image data. The quantitative results in Table 1 support the validity of our assumption, showing a mean relative deviation of up to 6.46% between pre- and post-operative anatomies.

Table 1. Deviation of pre- and postoperative ground truth anatomical models: Differences in diameter at sinutublar junction, valsava sinuses and aortic annulus are given in absolute values as well as relative to the postoperative measurement. Values of Mean and standard deviation are provided as well as 80-percentile and maximum.

	absolute (mm)			relative (%)		
measurement	mean (std)	80%	max	mean (std)	80%	max
sinutublar junction	2.3 (1.7)	3.7	5.7	6.46 (4.6)	10.5	14.9
valsava sinuses	1.1 (0.9)	1.7	4.1	3.49 (2.6)	5.2	9.98
annulus	1.5 (1.2)	2.5	5.2	5.06 (3.2)	7.7	14.3
point-to-mesh distance	1.6 (0.98)	2.4	2.8	-	-	-

5.2 Validation of In-Silico Implant Deployment

The validation of the in-silico implant deployment is performed on 20 patients with pre- and post-operative cardiac CT images, affected by various diseases such as calcific stenosis as mentioned in the previous section. It is important to note, that for this purpose the preoperative prediction result is compared with the real device imaged in the postoperative data, where the latter serves as a ground truth for this experiment.

The implant is virtually deployed into the associated anatomical model of the preoperative volume using the algorithm described in Sec 4.2. In the postoperative volume the ground truth implant is manually placed and fit to the imaged stent, which is well visible in image data, using a semi-automatic method based on the thin-plate-spline transformation. In the envisioned target application the optimal deployment location and orientation is manually selected by the clinician. For validation purposes this is indirectly available and has to be inferred by registering pre- and post-operative anatomical models. A selection of virtually deployed vs. their corresponding ground truth stents is depicted in Fig. 7. The performance is reported in Table 2 in terms of internal precision, by comparing only the virtual and real implants shape in isolation via symmetric point-to-point distance, and external precision. The latter means to compare the virtual and real implants position relative to clinically relevant locations, in order to account for the potentially critical conditions due to wrong implant sizing and placement such as blockage of coronary ostia and more importantly paravalvular leakages at the annular level as mentioned in Sec 1. This is done by computing the differences of the pre- and postoperatively measured distances from annulus ring and coronary ostia to the closest stent point respectively.

Table 2. Accuracy of in-silico valve deployment quantified from preop deployment prediction vs. postop ground truth stent and measured in mm: besides point-to-point distance, accuracy relative to the anatomies was estimated from the differences in distances between aortic valve annulus and coronary ostia and implant. Values of mean and standard deviation are provided as well as 80-percentile and maximum.

	mean (std)	80%	max
stent point-to-point	2.18 (1.77)	2.4	8.45
annulus	0.7 (0.73)	1.4	2.14
L coronary ostium	1.42 (1.51)	2.16	4.75
R coronary ostium	1.55 (1.24)	2.02	4.27

In the clinical context, the required accuracy is proportional to the tolerance between therapeutical alternatives. Considering the diameter differences of 3mm (at the annular level) of the Medtronic CoreValve implants (Sec 4.1), the system provides a sufficient approximation in at least 80% of the cases for prevention of paravalvular leakages, with an external accuracy of up to 1.4mm at the annular level. The algorithm performed at an average speed of 55sec on a standard desktop machine (Intel Xeon 2.66Ghz, 2GB RAM). Thus our framework enables for fast and efficient preoperative planning and risk minimization by finding the best implant type, size and deployment location and orientation via varying these parameters until optimal predicted performance is observed.

6 Discussion

In this paper a framework for computational decision support for percutaneous aortic valve implantation was presented. A fast and robust estimation of an anatomical model enables for precise modeling of the patient-specific morphology and is consequently used for in-silico implant deployment. The approach was validated with pre- and post-operative data sets from 20 patients and shows reasonable accuracy within the variation in appearance given by image and motion artifacts. To the best of our knowledge, this is the first time a computational framework is validated using real pre- and postoperative patient data. The framework is targeted for fast and efficient preoperative planning with a library of different implants, intraoperative guidance and postoperative assessment of interventional outcome. It may have impact on the cardiology of the future and improve the OR towards increased transparency.

References

1. Grube, E., Laborde, J., Gerckens, U., Felderhoff, T., Sauren, B., Buellesfeld, L., Mueller, R., Menichelli, M., Schmidt, T., Zickmann, B., Iversen, S., Stone, G.W.:

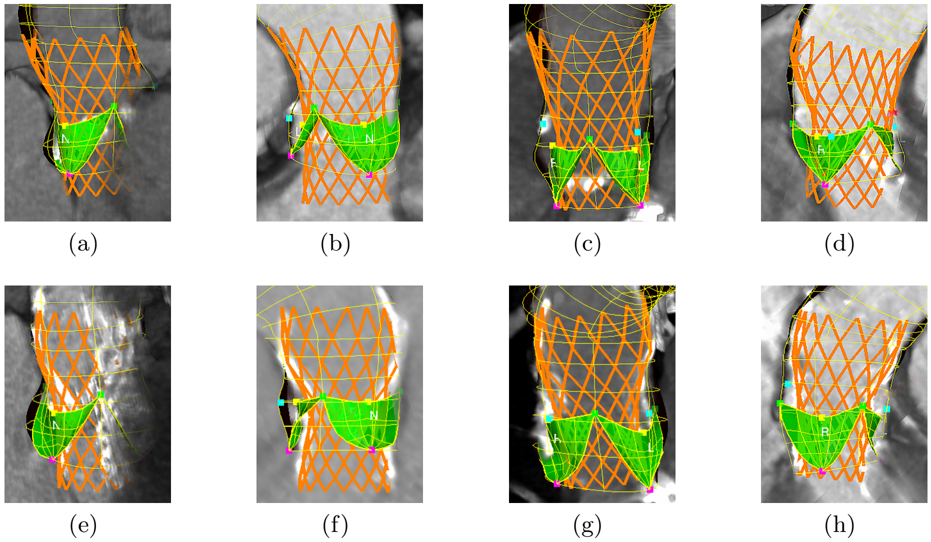

Fig. 7. Example results of preoperative virtual stent deployment (a-d) vs. postoperative ground truth stents (e-h) overlayed with with the anatomical models. Note the deviation of the virtually deployed stent around the sinutubular junction (upper end) in contrast to the close approximation at sinus and annular level, which is to due to the fact, that internal stiffness of the stent configuration is not modeled yet.

Percutaneous implantation of the corevalve self-expanding valve prosthesis in high-risk patients with aortic valve disease. Circulation (114) (2006) 1616–1624
2. Lloyd-Jones, D., et. al.: Heart disease and stroke statistics - 2009 update. Circulation (2009)
3. Otto, C., Bonow, R.: Valvular Heart Disease: A Companion to Braunwald's Heart Disease. Saunders (2009)
4. Grbic, S., Ionasec, R.I., Zheng, Y., Zaeuner, D., Georgescu, B., Comaniciu, D.: Aortic valve and ascending aortic root modeling from 3d and 3d+t ct. In: SPIE Medical Imaging, San Diego, USA (February 2010)
5. Ionasec, R.I., Voigt, I., Georgescu, B., Houle, H., Hornegger, J., Navab, N., Comaniciu, D.: Modeling and assessment of the aortic-mitral valve coupling from 4d tee and ct. In: Proc. MICCAI, London, USA (September 2009)
6. Zheng, Y., Georgescu, B., Ling, H., Zhou, S.K., Scheuering, M., Comaniciu, D.: Constrained marginal space learning for efficient 3d anatomical structure detection in medical images. In: CVPR. (2009) 194–201
7. Tu, Z.: Probabilistic boosting-tree: Learning discriminative models for classification, recognition, and clustering. In: Proc. ICCV, Washington, DC, USA (2005) 1589–1596
8. Larrabide, I., Radaelli, A., Frangi, A.F.: Fast virtual stenting with deformable meshes: Application to intracranial aneurysms. In: MICCAI (2). (2008) 790–797
9. Montagnat, J., Delingette, H.: 4d deformable models with temporal constraints : application to 4d cardiac image segmentation. Medical Image Analysis **9**(1) (February 2005) 87–100